Marine and Petroleum Geology 162 (2024) 106709

Contents lists available at ScienceDirect

Marine and Petroleum Geology

journal homepage: www.elsevier.com/locate/marpetgeo

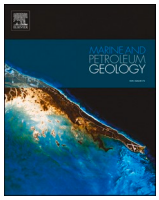

Diagenetic alterations induced by lamina-scale mass transfer and the impacts on shale oil reservoir formation in carbonate-rich shale of the Permian Lucaogou Formation, Jimusar Sag

Ke Li [a], Kelai Xi [a,*], Yingchang Cao [a], Xiang Shan [b], Miruo Lin [a]

[a] Key Laboratory of Deep Oil and Gas, China University of Petroleum (East China), Qingdao, 266580, China
[b] PetroChina Hangzhou Research Institute of Geology, Hangzhou, 310023, China

ARTICLE INFO

Keywords:
Carbonate-rich shale
Diagenetic alteration
Diagenetic mass transfer
Shale oil reservoir
Jimusar Sag

ABSTRACT

Diagenesis plays a crucial role in shale oil reservoir formation. However, complex organic-inorganic interactions result in pore system formation and heterogeneity changes at the centimeter, or even micrometer scale, which controls the evolution of shale oil reservoirs. In this paper, an integrated approach including core observation, thin section observation, cathodoluminescence thin section observation, scanning electron microscope, μ-XRF analysis, electron microprobe analysis, AMICS analysis, LA-ICP-MS analysis, and isotope analysis was used to clarify the laminae combination carbonate-rich shale, diagenetic alterations in different types of shale laminae and the controls on shale oil reservoir formation. According to the lamina combination, the carbonate-rich shale in the Permian Lucaogou Formation can be divided into three types. They are shale consists of dolomitic lamina and terrigenous felsic lamina (Type A shale), shale consists of calcite-rich tufaceous lamina and terrigenous felsic lamina (Type B shale) and shale consists of calcareous lamina and tufaceous lamina (Type C shale). Dolomite cementation is the major diagenesis in terrigenous felsic lamina of Type A shale. The dolomite can be identified as the early stage forming from recrystallization of micrite dolomite, and the late stage precipitate from adjacent dolomitic lamina. In the terrigenous felsic lamina of Type B shale, however, the calcite cementation is the dominated diagenesis, which was sourced from adjacent calcite-rich tufaceous lamina. Also, some feldspar dissolutions occurred in terrigenous felsic lamina during organic matter evolution. For the Type C shale, the main diagenetic alteration is micrite calcite recrystallization in calcareous lamina. The dissolution and precipitation of carbonate minerals between different laminae of carbonate-rich shale reveal that the organic matter evolution significantly influence the diagenetic alterations of inorganic minerals. Particularly, the diagenetic mass transfer and redistribution at the micro-scale in a relatively diagenetic system were confirmed by organic-inorganic interactions in laminated shale. In this process, dissolution pores and recrystallization pores have provided considerable reservoir pores for shale oil.

1. Introduction

With the increasing interest in unconventional oil and gas systems, shale oil and gas have shown great potential as an important role for future resources reserves worldwide (Zou et al., 2019; Zhao et al., 2020; Xu et al., 2022). However, due to the extremely heterogeneities and anisotropic nature of shale, identifying the “sweet spots” remains a major challenge during exploration and development (Hart et al., 2013; Hu et al., 2021). Reservoir pores formation and mechanical properties (brittleness) variation determine the likelihood that a shale will reserve and fracture (Yoon et al., 2020; Xu et al., 2022; Li et al., 2022; Gou and Xu, 2023), which are the basis of economically effective shale oil exploration. Previous studies have shown that deposition and diagenesis, as key controlling factors, determine the heterogeneities of the two properties (Hart et al., 2013; Milliken et al., 2016; Yoon et al., 2020; Jin et al., 2020). The deposition process determines the original heterogeneities of composition, structure, particle contact relationships, initial porosity, and organic matter abundance (Lazar et al., 2015; Wu et al., 2016; Zhang et al., 2022; Critelli et al., 2018; Civitelli et al., 2023; Criniti et al., 2023). Diagenetic alterations, such as carbonate cementation, carbonate recrystallization, silicate dissolution, clay mineral transformation, and thermal maturation of organic matter, usually result in

* Corresponding author.
E-mail address: kelai06016202@163.com (K. Xi).

https://doi.org/10.1016/j.marpetgeo.2024.106709
Received 29 November 2023; Received in revised form 10 January 2024; Accepted 15 January 2024
Available online 19 January 2024

heterogeneity changes at the centimeter, or even micrometer scale (Critelli and Nilsen, 1996; Liang et al., 2018; Han et al., 2020; Lin et al., 2021; Gou and Xu, 2023), directly affecting the properties of shale. However, shale usually present as complex components consisting of mixed deposits from terrestrial sources, endogenous sources, volcanic sources, and organic matter (Wu et al., 2016; Zhang et al., 2022). In addition, due to the fine particle size, frequent structural changes, low porosity and permeability, and complex compositions of shale, its diagenetic process involves complicated interactions among organic components, inorganic components, and pore systems (Schulz et al., 2016; Wu et al., 2017; Han et al., 2020). This complexity increases the difficulty of related studies. As a result, the evolution of shale diagenesis is still not fully understood.

Carbonate-rich shale is widely developed in lacustrine basins, and is one of the dominate reservoir rocks for shale oil (Liang et al., 2018; Li et al., 2022). As important mineral components in the rocks, carbonate minerals (calcite and dolomite) can cause changes in the micro-scale pore structure and mechanical properties (Mathia et al., 2016; Liang et al., 2018; Wang et al., 2021; Lin et al., 2021). The chemical properties of carbonate are sensitive to changes of diagenetic environment (Barbera et al., 2011; Caracciolo et al., 2014), which are prone to cementation, recrystallization, dissolution and metasomatism, making the diagenesis processes in carbonate-rich shale more complicated (Li et al., 2020). Carbonate minerals in shale present in various occurrences, such as biogenic debris, original micritic carbonate, carbonate veins, carbonate cements, recrystallized carbonates, or hydrothermal coarse-grained carbonates (Wang et al., 2018; Li et al., 2021; Dowey and Taylor, 2020). Their origin may be related to biogenesis, burial diagenesis, thermal evolutionary decarboxylation of organic matter, or exogenous carbonate-rich fluids (Dowey and Taylor, 2020; Li et al., 2020). During early diagenesis, algae, bacteria and other microbial activities can generate carbonate mineral, while biogenic debris are also prone to recrystallization towards carbonate minerals (Johannes and Puhan, 1971; Machel, 2001), while in the late stage of diagenesis, thermal decarboxylation of organic matter can release CO_2 and organic acids, promoting the dissolution of carbonate minerals and unstable Ca-rich minerals, leading to carbonate recrystallization and precipitation of authigenic carbonate minerals (Liang et al., 2018; Li et al., 2020). Thermal fluids rich in calcium can also lead to the precipitation of carbonate or directly carry carbonate clumps for deposition (Li et al., 2021). Numerous studies have shown that shale mainly occur as a closed diagenetic system (Liang et al., 2018; Lin et al., 2021; Zhang et al., 2023; Wang et al., 2023), and the formation of authigenic minerals follows the principle of mass balance (Cobbold et al., 2013; Milliken et al., 2016; Liang et al., 2018). Authigenic carbonate minerals in shales are often originated by organic-inorganic interactions at the laminated scale (Schulz et al., 2016; Wu et al., 2017; Li et al., 2020), however, the identification of different diagenesis and the mechanisms of mass transfer are not well understood, and there still exists a dispute on the mass transfer in thick shale during the diagenetic process.

The Permian Luchaogou Formation shale in the Jimusar Sag are mainly composed of carbonate, clay and feldspar-quartz minerals, with complex laminae combinations. The purpose of this paper is to study the organic-inorganic interaction process based on the different diagenesis within the laminae, and to gain insight into the mass transfer of mineral precipitation and dissolution processes in relatively closed diagenetic systems of shale. It is hoped that the research results can deepen the understanding of the diagenesis of carbonate-rich shale, so as to predict the characteristics of authigenic carbonate development and provides important guidance to shale oil exploration and development in study area.

2. Geological background

The Junggar Basin, located in northwestern China, is an important petroliferous basin, which can be subdivided into 6 sub-tectonic units of the Luliang uplift, the Wulungu depression, the Center depression, the West uplift, the South margin piedmont, and the East uplift (Fig. 1A). In the southwestern margin of the Eastern Uplift lies the Jimusar Sag, bounded by Santai fault in the south, Jimusar fault in the north, Xidi Fault and Laozhuangwan fault in the west, and Guxi uplift in the east (Fig. 1A), with an area of about 1278 km^2 (Wu et al., 2016). It is the result of multiple tectonic movements, including Hercynian movement, Indosinian movement, Yanshan movement, and Himalayan movement that occurred successively (Zhou et al., 2017). The Hercynian period is considered as the major stage for its formation, when intense tectonic subsidence during the late Early Permian led to deposition started in the sag as an independent unit. With the continuously intensified faulting around the sag, Fukang fault in the south, Shaqi bludge in the north and Guxi bludge in the east underwent different degrees of uplifting, and the embryo of Jimusar Sag was formed in the late Permian. Influenced by the followed Indosinian, Yanshan movement, the Jimusar Sag and its surrounding structural units subjected to different degrees of transformation. A slope higher in the east and lower in the west was formed in the Paleogene period, when the eastern part was generally uplifted higher than the western one. During the Himalayan period, the continued subduction of Bogurda Mountain in the south and intense uplifting of Fukang fault formed its present structural framework (Zhou et al., 2017).

The whole strata from the Permian to the Quaternary period was identified in the Jimusar Sag. However, due to the Indosinian and Yanshan movement, the Permian, Triassic, and Jurassic, and Cretaceous strata were eroded to different extents (Liu Y et al., 2019). The Lucaogou Formation (P_2l) widely distributed throughout the entire sag (Fig. 1B), with a thickness of 200–350 m. The formation recorded deposits from a saline lacustrine environment against the backdrop of intracontinental rifts (Liu Y et al., 2019). The intense volcanic activity around the sag provided a large amount of volcanic ash. A unique multi-component fine-grained sediment mixed with volcanic materials, terrigenous materials and carbonates were formed (Wu et al., 2016). The P_2l can be divided into two members: P_2l_1 and P_2l_2. The fine-grained sedimentary rocks include carbonate rocks, pyroclastic rocks, and terrigenous rocks (Fig. 1B), primarily consisting of laminated shale (Lin et al., 2021). In recent years, there has been a significant breakthrough in shale oil exploration in the P_2l of the Jimusar Sag. This has led to fine-grained sedimentary rocks becoming important research targets in oil exploration studies (Liu Y et al., 2019).

3. Databases and methods

About 300 core samples of P_2l formation were collected from the Xinjiang Oilfield Company, PetroChina. Among them, typical sample were chosen for microscope observation, cathode luminescene analysis (CL), scanning electron microscopy (SEM + EDS), micro X-Ray Fluorescence analysis (μ-XRF), AMICS analysis, EMPA analysis, microdrill sampling and stable strontium isotope analysis.

A total of 112 thin sections were prepared for this study. A Zeiss Axioscope A1 APOL digital transmission microscope with Image-Pro Plus software was used to analyze the lamination characteristics, the distribution of minerals and diagenetic alteration characteristics. Focused observations were made on the micro-morphology of grains, authigenic minerals and feldspar dissolution features. More precise analysis of high-resolution backscattered electron (BSE) images and mineral identification were used a scanning electron microscope (SEM) coupled with an energy-dispersive spectrometer (EDS) on 23 samples. Quantitative characteristics of minerals were determined by Advanced Mineral Identification and Characterization System (AMICS). From AMICS analysis, two-dimensional images showing reservoir rock mineral compositions and their spatial distribution can be obtained. Each image scanning was done using 20 nm resolution under the EDS probe for about 12 h. These samples were Pt-coated and observed under an SEM (Zeiss Crossbeam 550 FIB-SEM) at an acceleration voltage of 20 kV,

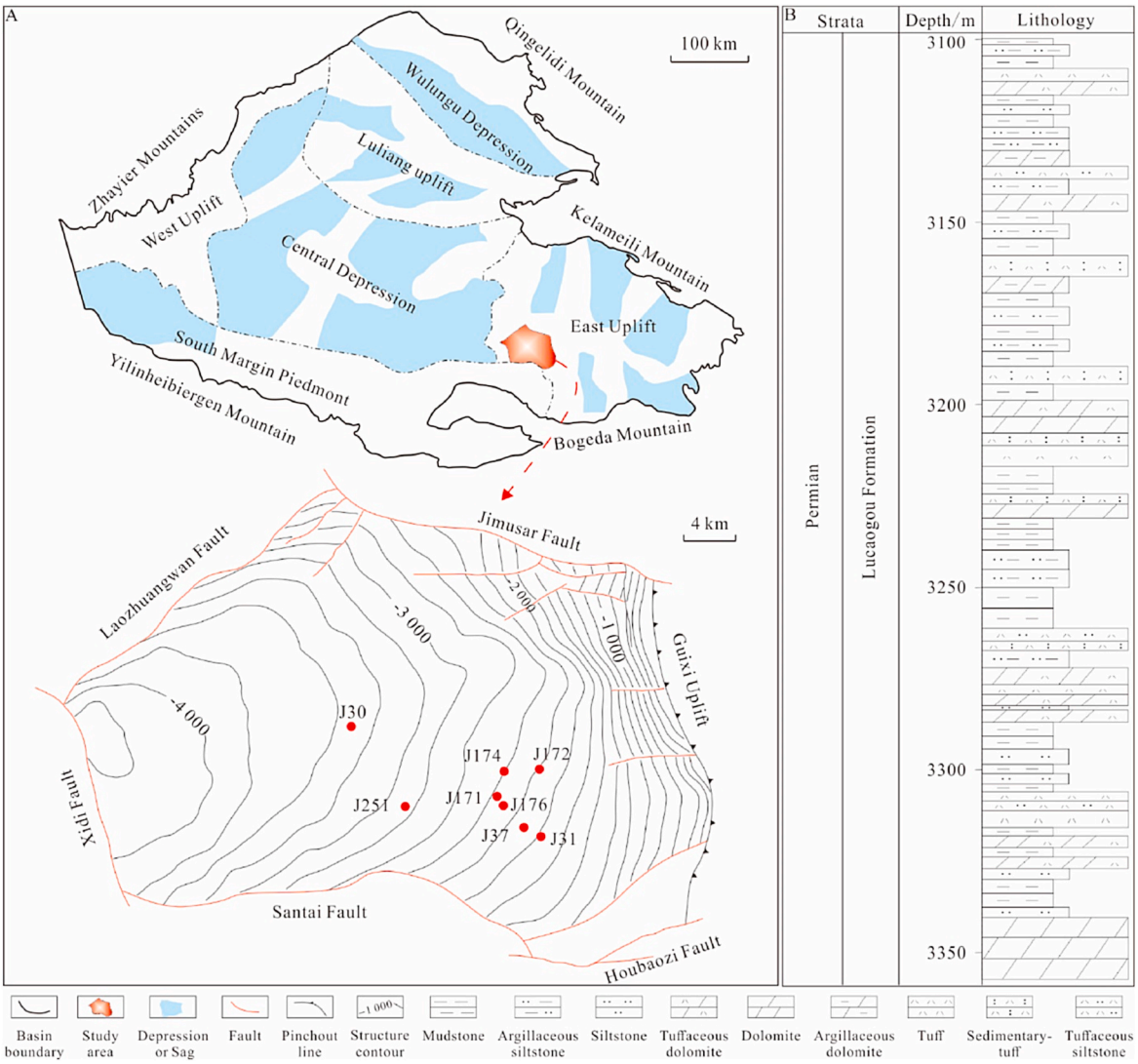

Fig. 1. (A) Structual location of the Jimusar Sag, structure contour and major wells of Lucaogou Formation; (B) Stratigraphic column of the Lucaogou Formation (modified from Qu et al., 2019).

with beam current of 1 nA. In addition, the element distribution characteristics of samples were clarified using high-precision element line scanning by EDS and μ-XRF.

Based on result of microscope observation, a total of 8 samples containing carbonate cement were chosen for cathode luminescene analysis (CL) using a Cambridge CL8200 MK5 detector equipped on the Zeiss microscope to identify the stages of carbonate. The samples were polished to thick sections, and CL images were collected at an acceleration voltage of 10 kV, beam current of 250 mA, and exposure durations of 10s (magnification 50·), 30s (magnification 100), and 60s (magnification 200·), respectively.

A total of 20 carbonate-rich shale samples were chosen for the electron probe microanalysis (EPMA) using a JXA-8230 instrument (JEOL) at an accelerating voltage of 20 keV and a beam current of 10 nA with a beam diameter of 1 μm. These thin-section samples were coated with Pt, and calcite and dolomite cement in different lamina were analyzed to identify chemical characteristics. The chemical results were accurate to within about 1 wt% for the major elements and 3 wt% for the trace elements.

To determine the origins of carbonate cements, 6 carbonate-rich samples were chosen for stable strontium, carbon and oxygen isotopes analysis. These samples were polished to thick sections first, a Micro-drilling (Bright MS-p120wh) with 2 μm bit was used to get calcite and dolomite cement in different lamina of shale. Carbon and oxygen isotope analysis was performed using a MAT-251EM gas stable isotope ratio mass spectrometer with resolution accuracies of $\delta^{13}C < 0.01‰$ and $\delta^{18}O < 0.02‰$. The Sr isotope test was completed using a NuInstru men multi-receiver inductively coupled plasma mass spectrometer (MC-ICP-MS), with an analytical precision of >0.004%.

The microscope observation, cathode luminescene analysis (CL), scanning electron microscopy (SEM + EDS), micro X-Ray Fluorescence analysis (μ-XRF), AMICS analysis, EMPA analysis, and microdrill sampling were performed in the Reservoir Geology and Basin Analysis Key Laboratory of the China University of Petroleum. The stable strontium, carbon and oxygen isotope analysis were performed in Chengdu University of Technology.

4. Results

4.1. Petrographic features

The shale of the Lucaogou Formation is highly heterogeneous and consists of various laminae with different compositions on the micron to millimeter scale. Based on the lamina combination, the shale can be classified into three types (Fig. 2A): Type A shale, which is composed of dolomitic laminae (DL) and terrigenous felsic laminae (TFL); Type B

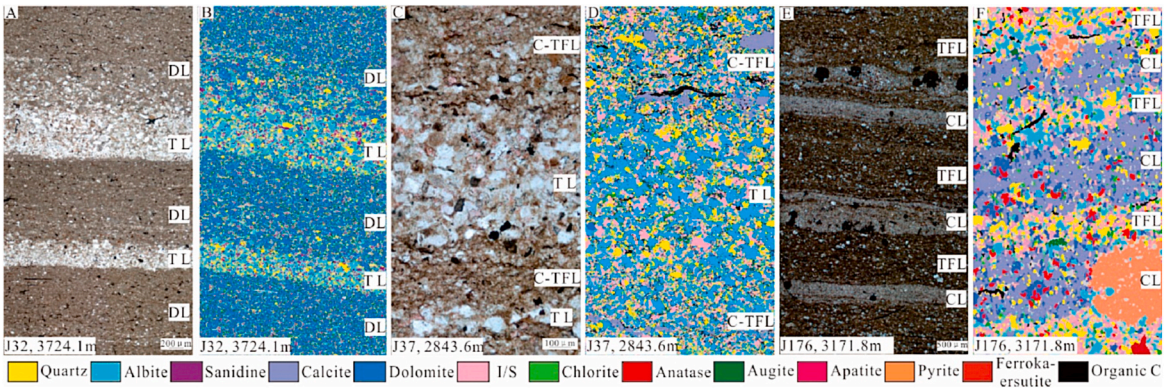

Fig. 2. Types and characteristics of shale of Lucaogou Formation in Jimusar Sag. (A) Photomicrographs of thin sections under plane-polarized light showing the characteristics of shale consisting of dolomitic lamina and terrigenous felsic lamina. (B) AMICS showing the characteristics of shale consisting of dolomitic lamina and terrigenous felsic lamina. (C) Photomicrographs of thin sections under plane-polarized light showing the characteristics of shale consisting of calcite-rich tufaceous lamina and terrigenous felsic lamina. (D) AMICS showing the characteristics of shale consisting of calcite-rich tufaceous lamina and terrigenous felsic lamina. (E) Photomicrographs of thin sections under plane-polarized light showing the characteristics of shale consisting of calcareous lamina and tufaceous lamina. (F) AMICS showing the characteristics of shale consisting of calcareous lamina and tufaceous lamina. DL = dolomitic lamina, TL = terrigenous felsic lamina, C-TFL = calcite-rich tufaceous lamina, TFL = tufaceous lamina, CL = calcareous lamina.

shale, which is composed of calcite-rich tufaceous laminae (C-TFL) and terrigenous felsic laminae (TL); and Type C shale, which is composed of calcareous laminae (CL) and tufaceous laminae (TFL). In terms of composition, all types of shales exhibit carbonate-rich characteristics.

Type A shale is primarily composed of dark dolomitic laminae and bright-colored silt-grained clastic laminae (Fig. 2A). The dark lamina is mainly composed of micrite spherule-like sedimentary dolomite, with a content exceeding 60%. It also contains some illite/smectite mixed layer (10.2%), albite (4.46%), and quartz (2.1%), etc. Some organic matter exists in this lamina, with an average content of about 2.3% (Table 1). The bright-colored lamina is primarily composed of minerals such as albite, sanidine, quartz, dolomite, I/S, mica, and rutile. However, the organic matter content is very low (Fig. 2B). Albite is the dominant mineral, comprising an average content of 40.07%, followed by quartz at 17.02% and sanidine at 12.8%. Dolomite is common in the lamina, occurring as intergranular cements, with an average total content of 11.8% (Table 1). Noticed, the roundness of quartz, feldspar, or fragment grains is mostly sub-angular to sub-rounded in the lamina, and some terrigenous deposition features, such as sequence bedding and erosion surface, were visible (Fig. 2A and B). Thus, the light lamina is called terrigenous felsic lamina.

Type B shale is mainly composed of dark clay laminae and bright-colored terrigenous felsic laminae (Fig. 2C). The dark lamina is primarily composed of I/S, with an average content of 63% (Table 1). Calcite is abundant in the lamina, appearing as lenticular or banded fragments, with an average content of about 10.3%. Quartz and albite are dispersed, comprising approximately 3.81% and 4.46% respectively. Other minerals, such as pyrite (0.14%), chlorite (0.12%), and apatite (0.1%), were also identified. Besides, there is abundant organic matter present in this lamina, with a total content is up to 8.65% (Fig. 2D). In the lamina, quartz and albite exhibit poor roundness with angular margins. This characteristic distinguishes it from terrigenous clastic sedimentation or the TL, but is similar to tuff or volcanic-exhalative hydrothermal deposition (Wu et al., 2016; Li et al., 2021; Li et al., 2023). The A1/Ti ratios of shales and silts typically exhibit similar values to those of their mother rock (Hayashi et al., 1997; Lin et al., 2021). XRF element analysis indicates that the Al/Ti ratio of the lamina (averaging 2.2) is significantly different from the shale terrigenous TL (averaging 6.5), suggesting distinct sources for the two laminae. Studies have shown that it is primarily derived from volcanic sources (Lin et al., 2021). The volcanic materials are easily transformed into clay minerals such as smectite and illite during burial processes (Campo et al., 2010), which is consistent with the current findings (Table 1). Therefore, the lamina is referred to as a calcite-rich tufaceous lamina. The bright-colored terrigenous felsic lamina is mainly composed of minerals such as albite (39.9%), sanidine (19.3%), quartz (13.4%), I/S (11.2%), mica (0.3%), etc (Fig. 2C and D, Table 1). Moreover, calcite is highly heterogeneous, with a content range of 0.25%–5.76%. It mostly occurs as cement filling pores.

Type C shale is mainly composed of dark clay laminae and bright-colored calcareous laminae (Fig. 2E). The dark clay-grained lamina is consistent with calcite-rich tufaceous lamina, containing I/S (60.5%),

Table 1
The mineral composition of the Lucaogou Formation shale.

Mineral	Type A shale		Type B shale		Type C shale	
	Content in TL	Content in DL	Content in TL	Content in C-TFL	Content in CL	Content in TFL
Quartz	17.02	2.10	13.40	3.81	5.09	6.10
Albite	40.07	4.46	39.90	4.46	5.72	9.40
Sanidine	12.80	1.94	19.30	2.46	0.00	1.26
Dolomite	11.82	67.30	0.00	0.00	10.30	4.70
Calcite	0.01	0.00	5.30	10.30	63.55	5.20
Pyrite	0.79	0.00	0.00	0.14	7.87	0.00
Mica	2.27	0.33	1.86	0.33	0.00	0.00
Ferrokaersutite	1.52	1.87	0.05	0.00	0.65	3.13
Apatite	0.00	0.00	0.00	0.10	0.00	1.90
Chlorite	0.05	0.02	1.08	0.12	0.00	0.00
I/S	5.77	10.20	11.08	63.30	1.53	60.50
Organic matter	0.00	2.30	0.00	5.60	0.08	3.65
Others	7.88	9.48	9.56	9.71	5.21	4.16

quartz (6.1%), albite (9.4%), dolomite (4.7%), and calcite (5.2%), etc (Fig. 2F, Table 1). The calcareous lamina is primarily composed of micrite calcite (more than 60%) and dolomite (10.3%). Pyrite is common, with an average content of 2.87% and a maximum content of 9.72%. Other minerals such as quartz (5.09%), albite (5.72%), and phosphorus-rich minerals (1.9%) were also identified (Fig. 2F, Table 1).

Overall, all three types of shale show carbonate-rich characteristics. Type A shale is rich in dolomite, mainly presenting as sedimentary micrite dolomite in the DL, and dolomite cement in the TL. Type B shale is rich in calcite, which occurs as calcareous fragments in the C-TFL, and as calcite cement in the TL. Type C shale is also rich in calcite, and are composed of sedimentary micrite calcite and authigenic sparry calcite, primarily found in the CL.

4.2. Dolomite authigenesis

Authigenic dolomite is the main diagenetic mineral in Type A shale. Two types of authigenic dolomite were identified, occurring as dolomite cement and recrystallized dolomite (Fig. 3A). The dolomite cements generally develop in the TL, with an average content of 7.33% (Fig. 3A and B). SEM analysis shows that the crystal of dolomite cement is more euhedral than micrite dolomite in the shale, being irregularly angular to sub-round (Fig. 3C). Furthermore, the dolomite cements were primarily distributed in intergranular pores, with smaller amount filling the feldspar dissolution pores (Fig. 3C). Under cathodoluminescence, the dolomite cements can be clearly divided into two stages. The inner core (stage I) exhibits non-luminescence or dark orange luminescent colors, and the outer rims (stage II) display bright yellow luminescent colors (Fig. 3D). BSE analysis shows a clear boundary between the two stages of dolomite. The stage I dolomite is generally brighter without intergranular pores, while the stage II dolomite is darker and has a significant number of intergranular pores developing along the boundary (Fig. 3C). Elemental analysis shows that the concentrations of Na, K, Si, Al, and Fe are higher in stage II dolomite, while the concentrations of Sr and Mg are significantly higher in stage I dolomite (Fig. 4A). The isotope ratio of $^{86}Sr/^{87}Sr$ is lower, with a value of 0.7053. For the recrystallized dolomites, they mainly developed adjacent to organic matter in DL of Type A shale (Fig. 3E). Their characteristics are similar to dolomite cements in TL, however, the difference is that recrystallized dolomites are more homogeneous without outer rims (Fig. 3E). In addition, it was also observed that some recrystallized dolomite, which developed adjacent to micrite dolomite, occurred in TL (Fig. 3C).

4.3. Calcite precipitation

Authigenic calcites, which is observed as calcite cement and silty-crystal calcite (Fig. 5), are common in Type B shale. Calcite cements generally developed in TL, primarily in feldspar dissolution pores, and rarely filling intergranular pores (Fig. 5A–C). The content of calcite cements is heterogeneous in different TL, with a distribution ranging from 0.25% to 5.76%. Notably, calcite cements are more enriched in proximity to the C-TFL, which is richer in calcareous fragments. Under cathodoluminescence, the calcite cements exhibit only a bright yellow color (Fig. 5D), and appear to be more concentrated near the interface of two laminae in certain thicker TL (Fig. 5D). Elemental analysis shows calcite cements are rich in FeO, MgO, and contain many impurity elements such as K_2O and SiO_2 (Fig. 4B). Moreover, they exhibit a higher $^{86}Sr/^{87}Sr$, with a value of 0.7097. In the C-TFL, a large amount of silty-crystal calcite was observed. The silty-crystal calcites are irregular in morphology, banded or lenticular, and often surrounded by organic matter (Fig. 5E). Obvious dissolution has developed in these calcites, which contain numerous intergranular pores (Fig. 5E). Elemental analysis shows that silty-crystal calcites contain lower levels of SiO_2, MgO, SrO, and K_2O compared to calcite cements (Fig. 4B). However, they also exhibit a higher ratio of $^{86}Sr/^{87}Sr$, with a value of 0.70869.

4.4. Calcite recrystallization

In Type C shale, calcite recrystallization commonly occurred near two types of laminae interfaces, resulting in silty-crystal calcites (Fig. 6A

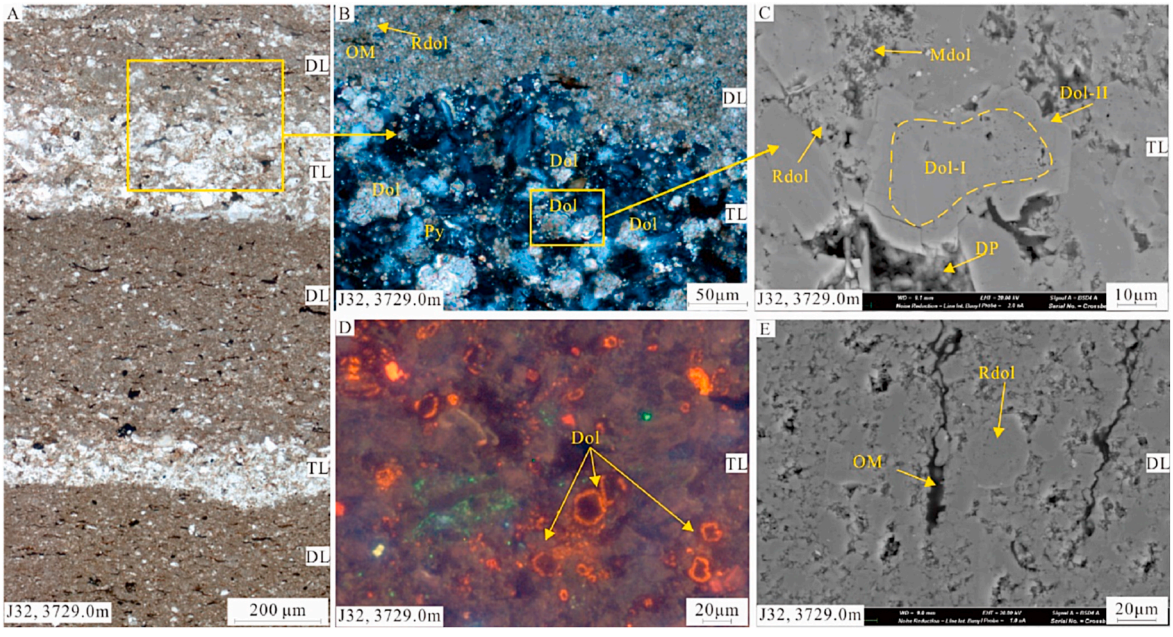

Fig. 3. Types and characteristics of diagenesis in the shale consisting of dolomitic lamina (DL) and terrigenous felsic lamina (TL). (A) Photomicrographs of thin sections showing Type A shale. (B) Photomicrographs of thin sections under orthogonal light showing dolomite cement and recrystallized dolomite in type A shale. (C) BSE image showing the dolomite cements were mainly distributed in intergranular pores of TL laminae, and a clear boundary occurred between the two stages of dolomite; (D) Cathode luminescence (CL) photomicrographs demonstrating that dolomite cement can be obviously divided into two stages, with the inner core (stage I) being non-luminesence or dark orange luminescence colors, the outer rims (stage II) being bright yellow luminescence colors; (E) BSE image showing recrystallized dolomite developed near organic matter in dolomitic lamina. DL = dolomitic lamina, TL = terrigenous felsic lamina, OM = organic matter, Rdol = recrystallized dolomite, Mdol = micrite dolomite, DP = dissolution pore, Dol-I = = stage I dolomite, Dol-II = stage II dolomite.

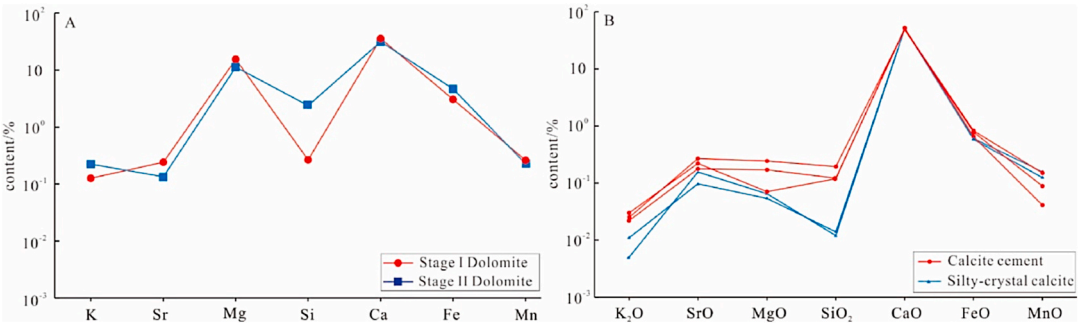

Fig. 4. (A) Elemental geochemistry of the two types of dolomites in Type A shale; (B) Elemental geochemistry of the two types of calcites in Type B shale.

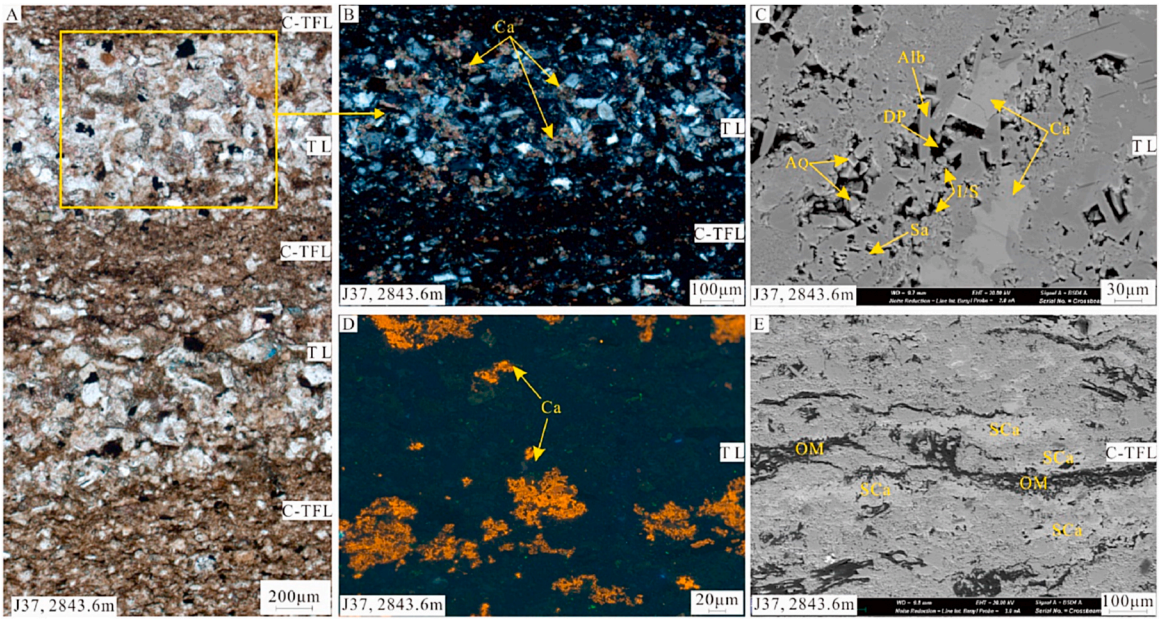

Fig. 5. Types and characteristics of diagenesis in the shale consisting of calcite-rich tufaceous lamina (C-TFL) and terrigenous felsic lamina (TL). (A) Photomicrographs of thin sections showing Type B shale. (B) Photomicrographs of thin sections under orthogonal light showing calcite cements in terrigenous felsic lamina. (C) BSE image showing calcite cements, authigenic albites, authigenic quartz, some illite and chlorite developed in the dissolution pores of Sanidine. (D) CL photomicrographs demonstrating that calcite cements have bright yellow luminescent color. (E) BSE image showing a large amount of silty-crystal calcite developed near organic matter in calcite-rich tufaceous lamina and obvious dissolution pore developed in silty-crystal calcite. TL = terrigenous felsic lamina, C-TFL = calcite-rich tufaceous lamina, Ca = calcite cements, Alb = authigenic albites, AQ = authigenic quartz, DP = dissolution pores, Alb = authigenic albites, I/S = Illite/Smectite, Sa = Sanidine, SCa = silty-crystal calcite.

and B). The silty-crystal calcites are more euhedral than micrite sedimentary calcite, with irregularly angular to rhombic grain morphology (Fig. 6B). In addition, aggregates composed of multiple recrystallized calcites were observed near the boundaries of two laminae. These aggregates were associated with pyrite and organic matter, forming a coexisting combination (Fig. 6C). The intercrystalline pores in the aggregates are abundant and are commonly filled with bitumen (Fig. 6C). In addition, numerous pyrite aggregates and minerals enriched in P (mainly composed of calcium phosphate) were found near the silty-crystal calcites (Fig. 6D). The morphology and size of the pyrite vary, with a content ranging from 1.25% to 12.7% and an average content of 5.05%. The individual crystals of P-enriched minerals are extremely small hexagonal prisms, with some crystals having a perfect hexagonal cross-section (Fig. 6D and E). Similar features were observed near the organic matter in the TFL (Fig. 6E). Recrystallized calcites also developed near organic matter in the TFL (Fig. 6E). Elemental analysis shows that silty-crystal calcites have lower Si, Al, Na, K, and Mg contents than micrite calcites (Fig. 7A). However, the REE analysis results show that the two types of calcite have similar characteristics. They exhibit a rightward trend, indicating light rare earth enrichment distribution patterns (Fig. 7B). Moreover, two types of calcite also show a lower $^{86}Sr/^{87}Sr$ ratio, with a value of 0.7058.

5. Discussions

5.1. Lamina-scale diagenetic mass transfer and the related diagenesis

5.1.1. The diffusion of calcium and magnesium rich fluid resulted in dolomite precipitation

Dolomite cements are the dominant diagenetic minerals in type A shales, generally developing in the TL. Two stages of dolomite cements are identified, with Stage I (inner core) exhibiting non-luminescence or dark orange luminescent colors, while Stage II (outer rims) occurs as bright yellow luminescent colors (Fig. 3). Based on BSE analysis, dolomite cements mostly fill the intergranular pores and rarely fill feldspar dissolution pores (Fig. 3C). This indicates that they were primarily formed before feldspar dissolution. EDS scanning analysis shows that dolomite cements were commonly adjacent to micritic dolomite in the TL (Fig. 8A and B). The micrite dolomites are homogeneously distributed in intergranular pores and have similar characteristics to micrite

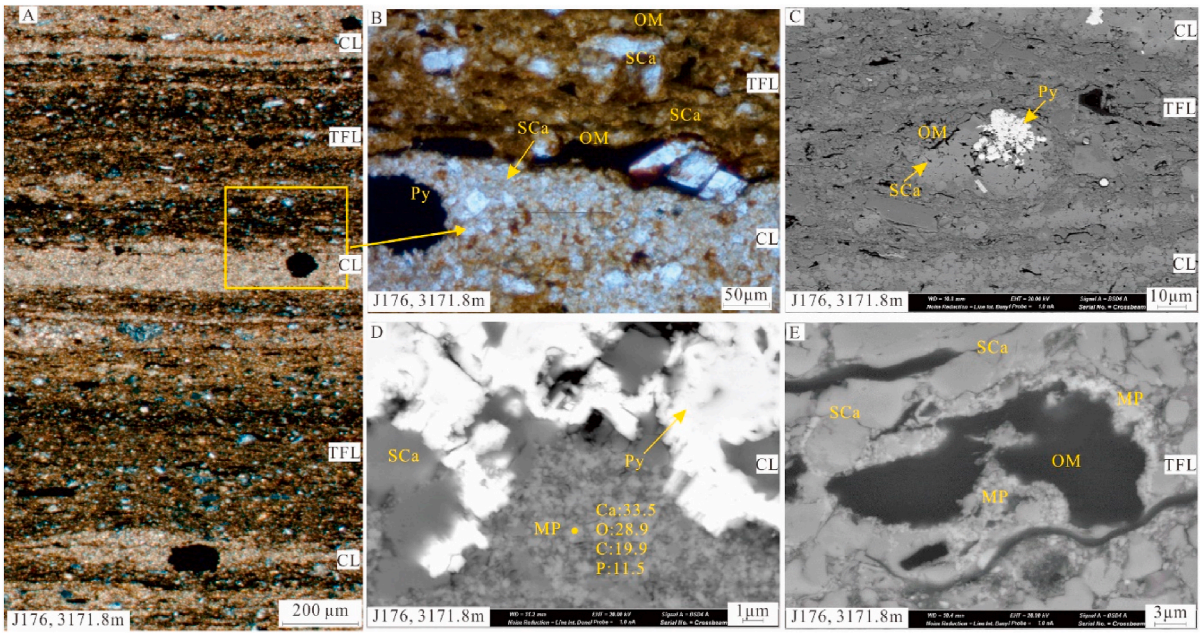

Fig. 6. Types and characteristics of diagenesis in the shale consisting of calcareous lamina (CL) and tufaceous lamina (TFL). (A) Photomicrographs of thin sections showing Type B shale. (B) Photomicrographs of thin sections under orthogonal light showing silty-crystal calcites near the laminae interface and massive pyrite. (C) BSE image showing aggregates composed of multiple recrystallized calcites, massive pyrite and organic matter; (D) BSE image showing minerals enriched in P, organic matter, and pyrite aggregates adjacent to the silty-crystal calcites, and the silty-crystal calcites were replaced by pyrite in some place; (E) BSE image showing minerals enriched in P and silty-crystal calcites adjacent to the organic matter. TFL = tufaceous lamina, CL = calcareous lamina, Py = pyrite, OM = organic matter, SCa = silty-crystal calcites, MP = minerals enriched in P.

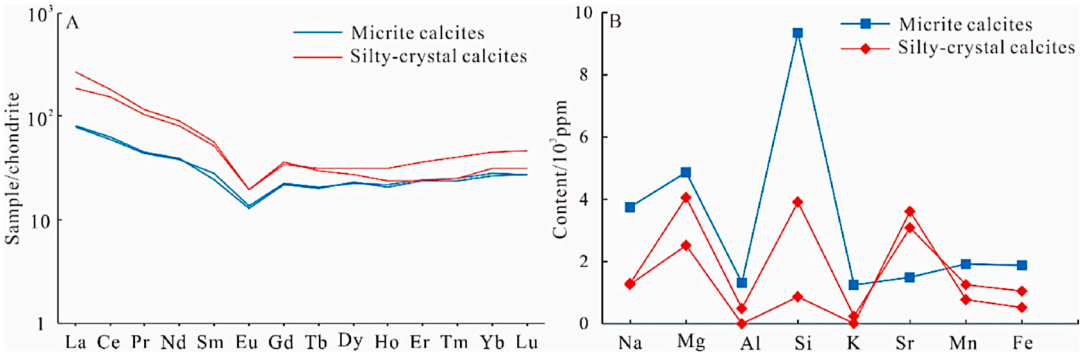

Fig. 7. Elemental geochemistry of the two types of calcite in Type C shale. (A) Rare earth enrichment distribution patterns of two types of calcites; (B) Element characteristics of the two types of calcites.

dolomite in the DL (Fig. 3A). Many sparry dolomites are observed in the micrite dolomites (Fig. 8C), and their characteristics are similar to Stage I dolomite. In the DL, some similar recrystallized dolomites developed adjacent to organic matter (Fig. 3E). Elemental analysis shows that the compositions of Stage I dolomites are similar to those of recrystallized dolomites. They are relatively richer in Mg and Sr, and have lower ratios of Ca/Mg, Fe/Mg, and Fe/Mn (Fig. 9). Therefore, Stage I dolomites are interpreted as originating from the recrystallization of micritic dolomite in the TL. Previous studies have shown that the reaction of micritic dolomite with organic acids and CO_2 only results in a dissolution-reprecipitation reaction (Edery et al., 2011; Wu et al., 2017; Li et al., 2019). This reaction transforms micritic dolomite into stable and larger sparry crystal dolomite, without any precipitation of other minerals occurring (Wu et al., 2017). The reaction equation of interest can be expressed as:

$$CO_2+H_2O=H^+ + HCO_3^-$$

$$CaMg(CO_3)_2 + 2H^+ \leftrightarrow Ca^{2+} + Mg^{2+} + 2HCO_3^-$$

Stage II dolomites occur as rims of Stage I dolomite (Fig. 3C and D). In some TL, similar dolomite rims were observed on the outside of carbonate fragments (Fig. 8D). EMPA analysis shows that the elements of stage II dolomites are also consistent with those of the carbonate fragment rims (Fig. 9). It is suggested that Stage II dolomites were formed through the continued precipitation of dolomite around stage I dolomite. Unlike Stage I dolomites, Stage II dolomites are significantly more enriched in K, Si, Al, and Fe (Fig. 9). This indicates that the pore fluid was rich in these elements during Stage II dolomite precipitation. According to BSE and EDS analysis, a significant quantity of Ca-rich sanidines is in the TL (Fig. 8E), and these sanidines typically exhibit weak dissolution. The dissolution of feldspar can provide sources such as Ca, K, Al, Si for the precipitation of Stage II dolomite. However, the weak dissolution of feldspar is unlikely to yield a sufficient concentration of relevant ions. High-precision element line scanning results show that the concentrations of Ca and Mg ions in the DL decrease as the distance from the interface of the two laminae (Fig. 10). This indicates that these ions diffused from the DL to the TL. A lot of illite or I/S were observed in the

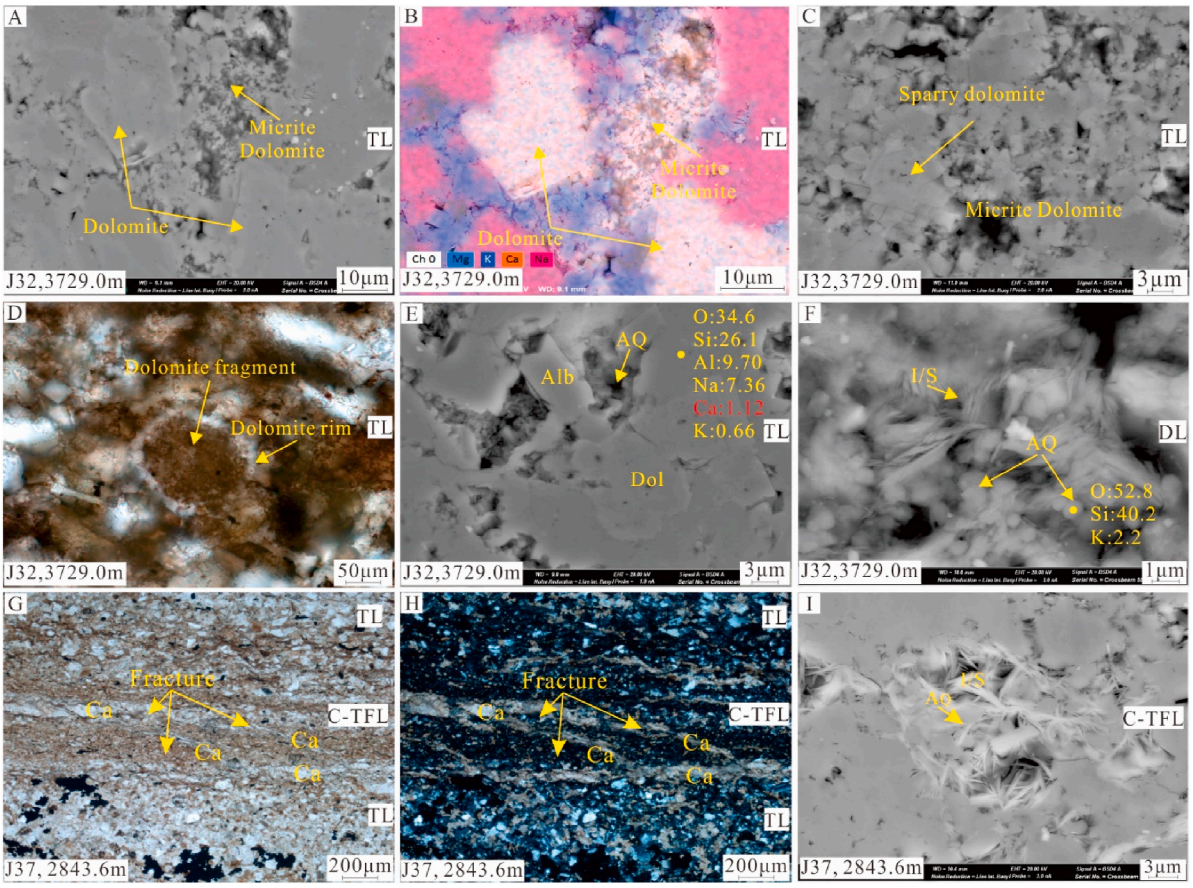

Fig. 8. Characteristics of dolomite cements and calcite cements in type A and type B shale. (A) Backscattered electron (BSE) image showing dolomite cements were mostly filled in the intergranular pores and commonly developed adjacent to micritic dolomite. (B) EDS scanning showing that dolomite cements commonly developed adjacent to micritic dolomite. (C) BSE image showing sparry dolomites developed in the micrite dolomites of TL. (D) Photomicrographs of thin sections under plane-polarized light showing dolomite rims developed on the outside of carbonate fragments. (E) BSE image showing weak dissolution of Ca-rich sanidines, and authigenic albites developed in the dissolution pores. (F) BSE image showing some authigenic micro-quartz filled in the intercrystal pore of I/S, indicating illitization occurred in CL of type A shale. (G) Photomicrographs of thin sections under plane-polarized light showing calcite developed in the micro-fracture connecting the two types of laminae, and stronger calcite cementation occurred in the TL near the microcracks in type B shale. (H) Photomicrographs of thin sections under orthogonal light showing the same areas with (H). (I) BSE image showing some authigenic micro-quartz filled in the intercrystal pore of I/S, indicating illitization occurred in C-TFL of type B shale. DL = dolomitic lamina, TL = terrigenous felsic lamina, C-TFL = calcite-rich tufaceous lamina, TFL = tufaceous lamina, Alb = albite, AQ = authigenic quartz.

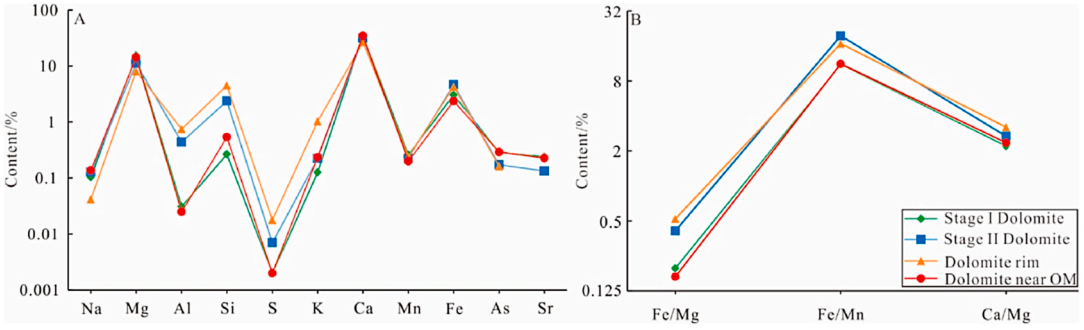

Fig. 9. Elemental geochemistry of the two types of dolomite in the shale consisting of dolomitic lamina (DL) and terrigenous felsic lamina (TL).

DL (Fig. 8F), and some authigenic micro-quartz developed in the intercrystalline pores of clay minerals (Fig. 8F), suggesting that illitization commonly occurred (Yang et al., 2018; Jin et al., 2020; Lin et al., 2021). During this process, certain ions such as Si^{4+}, Al^{3+}, Mg^{2+}, and Fe^{2+} can be released into the pore water, serving as a source of materials for the formation of stage II dolomites (Wu et al., 2017; Sun et al., 2020). In summary, the micrite dolomite in the TL is of sedimentary origin, while the dolomite cement was formed during diagenesis. Dolomite cement is believed to undergo two stages. During the thermal evolution of organic matter, the organic acids and CO_2 generated by the organic matter were released from the DL into the TL. The micritic dolomite of sedimentary origin in the TL preferentially underwent dissolution-reprecipitation reactions (Wu et al., 2017) and transformed into Stage I dolomite. As the organic matter continued to mature, a large amount of organic acids, along with Ca and Mg rich fluid, infiltrated the TL. The excessive organic acids started dissolving the feldspar, and the smectite transformed into

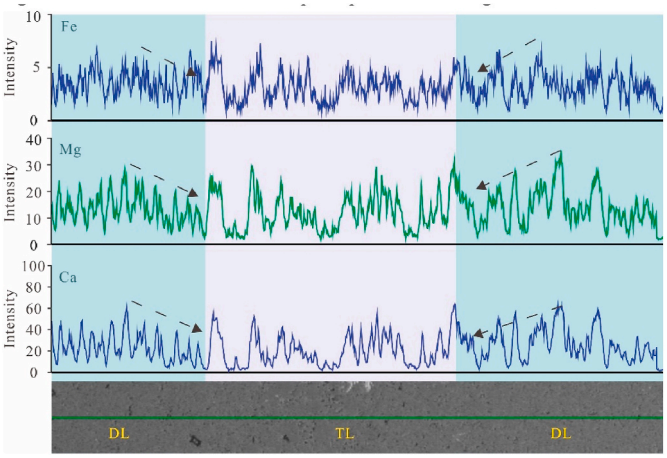

Fig. 10. Distribution characteristics of elements in the shale consisting of dolomitic lamina (DL) and terrigenous felsic lamina (TL) by line scanning.

illite, providing a source of material for the precipitation of stage II dolomite.

5.1.2. The diffusion of calcium-rich fluid resulted in calcite precipitation

Calcite cements primarily occurred in the TL of type B shales, and cathodoluminescence analysis reveals that there is only one stage of calcite cements (Fig. 5). In the adjacent C-TFL, abundant silty-crystal calcites were identified near the organic matter (Fig. 5E). AMICS analysis shows that the content of calcite cements increases with silty-crystal calcites in adjacent C-TFL laminae (Fig. 11A). Moreover, μ-XRF analysis also show that the Ca concentrations of the TL are more enriched near the C-TFL (Fig. 12). In some TL, there is a trend where calcites decrease away from the interface between two laminae (Figs. 5D and 12). Authigenic calcites were also observed in the micro-fracture connecting the two types of laminae, and stronger calcite cementation occurred in the TL laminae near the microcracks (Fig. 8G–H). These phenomena indicate that the calcite cements in TL originated from silty-crystal calcites in adjacent C-TFL.

According to elemental analysis, calcite cements have similar chemical compositions to the silty-crystal calcites (Fig. 4B). Their $^{87}Sr/^{86}Sr$ isotopic values also show similarities, ranging between 0.7085 and 0.7010 (Fig. 11B). These values are clearly distinct from other types of carbonates found in the Lucaogou formation shale (Li et al., 2021). The $\delta^{13}C$ isotope of calcite cements shows extremely high positive values ranging from 2.8‰ to 3.1‰, indicating an inorganic source of carbon (Tobia, 2018; Xi et al., 2019). This supports the idea that the calcite cements originated from early carbonate. High-precision element line scanning results show the concentration of Ca ions in the C-TFL

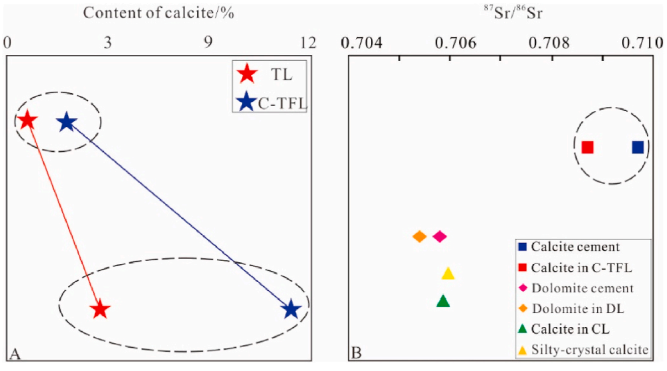

Fig. 11. (A) Content of calcite cements in different TL of shale consisting of calcite-rich tufaceous lamina (C-TFL) and terrigenous felsic lamina (TL); (B) $^{87}Sr/^{86}Sr$ isotopic characteristics of carbonates.

decreases as the distance from the interface of the two laminae decreases (Fig. 13). This also indicates Ca ions were diffused from the C-TFL to the TL. During this process, by-products of the thermal conversion of organic matter in the C-TFL may promote calcium carbonate precipitation (Mathia et al., 2016; Liang et al., 2018; Dowey and Taylor, 2020).

However, the calcite cement has higher concentrations of K, Si, Fe, Mg, and Sr compared to the silty-crystal calcites (Fig. 4A). Previous studies have shown that the composition of carbonate cements is influenced by changes in diagenetic fluids (Parcerisa et al., 2006; Caracciolo et al., 2014; Li et al., 2020). Therefore, calcite forms when the pore water environment contains higher concentrations of these elements. In the TL, the dissolution of sanidines was common, and the resulting products, including albite, quartz, and I/S, precipitated nearby within the lamina (Fig. 5C). There is only one stage of calcite cements, which mostly filled in feldspar dissolution pores (Fig. 5C). This indicates that they were formed after the dissolution of sanidines. During the dissolution process of sanidines, cations such as K^+ and Si^{4+} were able to be released into the pore fluid (Thyne et al., 2001; Yuan et al., 2019; Lin et al., 2021). These cations can serve as a source for the formation of later calcite cements. This is supported by the correlation that the K_2O content increases with the increasing SiO_2 content of calcite cements (Fig. 14A). In addition, there are positive correlations between the contents of FeO, MgO, and SrO (Fig. 14B–D). In the C-TFL, a significant transformation of smectite to illite occurred (Fig. 8I). This process will result in the release of more Fe, Mg, and Sr into the pore water (Stroker et al., 2013; Sun et al., 2020; Lin et al., 2021). These ions can accompany organic acids and carbonate-rich fluid discharging from the C-TFL to the TL (Fig. 11), providing a source of the material for the precipitation of calcite cements (Dowey and Taylor, 2020). This opinion was supported by similar chemical composition characteristics in calcite cements and calcite in micro-fractures, showing higher concentrations of Mg, Fe, and Sr ions (Fig. 11). In summary, the organic matter in the C-TFL matured as the temperature increased, leading to the release of organic acids during the burial process (Liang et al., 2018; Liu H et al., 2019; Lin et al., 2021). These organic acids then dissolved the sedimentary calcites, resulting in the formation of pore fluids rich in carbonate. Simultaneously, the transformation of smectite to illite in the C-TFL provided a large number of ions. The pore fluids rich in carbonate were released into the adjacent TL through micro-fractures, resulting in the formation of calcite cements. Moreover, the dissolution of sanidines in TL provided a material source. The potassium ions generated from the dissolution of sanidines diffused into the surroundings, facilitating the conversion of smectite into illite (Fig. 8I), and providing some ions for the formation of calcite cement, authigenic albite, and quartz (Fig. 5C).

5.1.3. The diffusion of organic acids resulted in calcite recrystallization

Calcite recrystallization is common in the shales of the Luchaogou Formation. It mainly occurred near organic matter or the organic-rich lamina, especially in type C shale. In type C shale, the TFL are rich in organic matter, and the micrite calcite of the CL near the laminae interface underwent widespread recrystallization (Fig. 6). The calcites near the organic matter within the TFL laminae also show a similar phenomenon (Fig. 6E). Element analysis shows that the micrite calcites and silty-crystal calcites in the CL have similar REE distribution patterns (Fig. 7A), indicating a common origin (Li et al., 2021). Under high-precision SEM, it was observed that silty-crystal calcites are composed of multiple micrite calcite (Fig. 15A), and dark areas containing impurity minerals with higher content of Si, Na, Al, and other elements were also present (Fig. 15B). Large amounts of related ions are also found in the micrite calcite (Fig. 15C), indicating that silty-crystal calcites were formed through the recrystallization of micrite calcites in the CL (Liang et al., 2018; Liu H et al., 2019). Furthermore, the concentrations of Mg, Al, Si, and other elements in the micrite calcite are significantly higher than those in silty-crystal calcites (Fig. 7B). This suggests that the silty-crystal calcites became more pure during the recrystallization process. Elemental analysis of individual silty-crystal

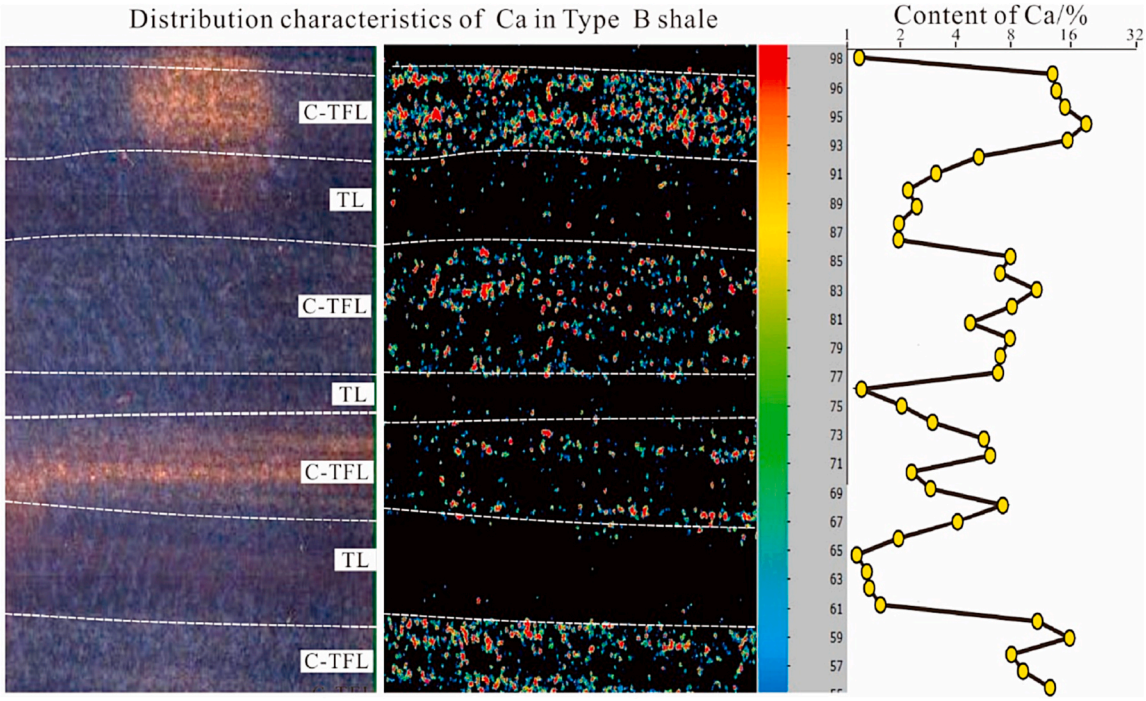

Fig. 12. Distribution characteristics of calcium in the shale consisting of calcite-rich tufaceous lamina (C-TFL) and terrigenous felsic lamina (TL).

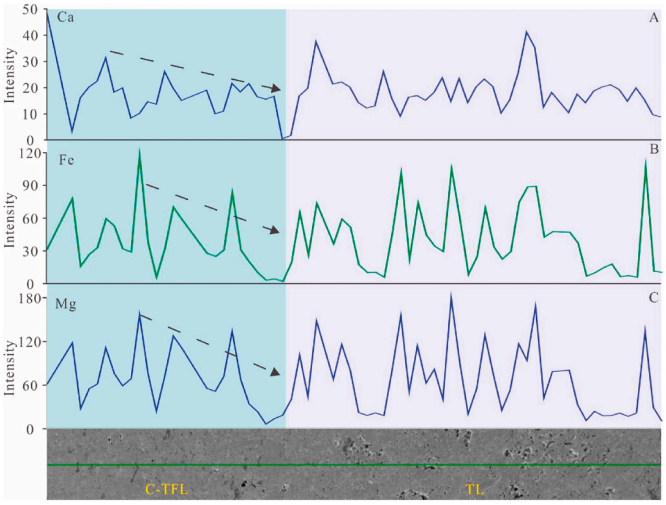

Fig. 13. Distribution characteristics of elements in the shale consistings of calcite-rich tufaceous lamina (C-TFL) and terrigenous felsic lamina (TL) by line scanning.

calcite also shows that the content of Mg decreases from the inside out, and the Ca/Mg ratio increases (Fig. 16). This indicates that Mg gradually decreased in the pore fluid during recrystallization. Mg, Al, and Si are easily incorporated into the calcite lattice, hindering the growth of calcite crystals (Reddy, 2012; Liang et al., 2018). Studies have shown that during the recrystallization of calcite, organic fluids can remove toxic or impure ions from calcite, thereby facilitating the growth of calcite (Reddy, 2012; Liang et al., 2018). Therefore, Mg ions continuously migrate out from the CL, causing the transformation of micrite calcite into silty-crystal calcite, and the organic acids generated by organic matter evolution in the TFL trigger this process. High-precision element line scanning results show that the concentration of Mg decreases as the distance from the calcite lamina decreases (Fig. 17), confirming the loss of ions.

Moreover, numerous pyrite aggregates were found near the silty-crystal calcites (Fig. 6B and C). Massive pyrite is another common mineral in type C shale and often coexists with P-rich minerals (Fig. 15D and E). It is typically surrounded by organic matter (Fig. 15D and E). P is a common constituent of biological materials (Xiong et al., 2019), and the abundance of P-bearing bioclasts near organic matter suggests that massive pyrite may be related to the evolution of organic matter (Fig. 6E). The organic matter of type C shale is enriched in S (0.184%), which could provide a source for pyrite. The TFL adjacent to the CL likely acted as a source of pyrite, as the conversion of smectite to illite produced ample sources of iron that migrated towards the pyrite near the interfaces (Fig. 15F). High-precision element line scanning results indicate that the Fe content in the TFL increases as the distance from the interface increases (Fig. 17), supporting the migration of Fe. It's worth noting that the formation of pyrites appears to facilitate the recrystallization of micrite calcite into silty-crystal calcites. Evidence includes the observation of silty-crystal calcites adjacent to the massive pyrites in the CL, as well as clusters of multiple recrystallized calcites associated with pyrites and organic matter near the interface of two laminae (Fig. 6B–D). Pyrites promote the degradation of organic matter and the generation of CO_2 (Lai et al., 2016; Lin et al., 2021), thereby facilitating the recrystallization of micrite calcite into larger calcite crystals. With increased burial depth, the thermal maturation of organic matter in the TFL will generate acidic fluids such as CO_2 and HS^-, which resulted in the dissolution-precipitation of micrite calcite (Liang et al., 2018; Liu H et al., 2019). Furthermore, the illitization of smectite in the TFL resulted in the generation of numerous ions (Stroker et al., 2013; Sun et al., 2020). This diluted the concentration of Mg ions, which in turn facilitated the recrystallization of micrite calcites into silty-crystal calcites (Reddy, 2012). Simultaneously, the high HS^- content in the degradation of sulfur-rich organic matter promoted the formation of massive pyrites (Khan et al., 2022). Thus, the formation of massive pyrite and recrystallized calcites was mutually complementary, resulting in the presence of pyrite and recrystallized calcite associated with organic matter.

5.2. *Impacts on shale oil reservoir formation*

Shale mainly occurs as a closed diagenetic system, in which organic

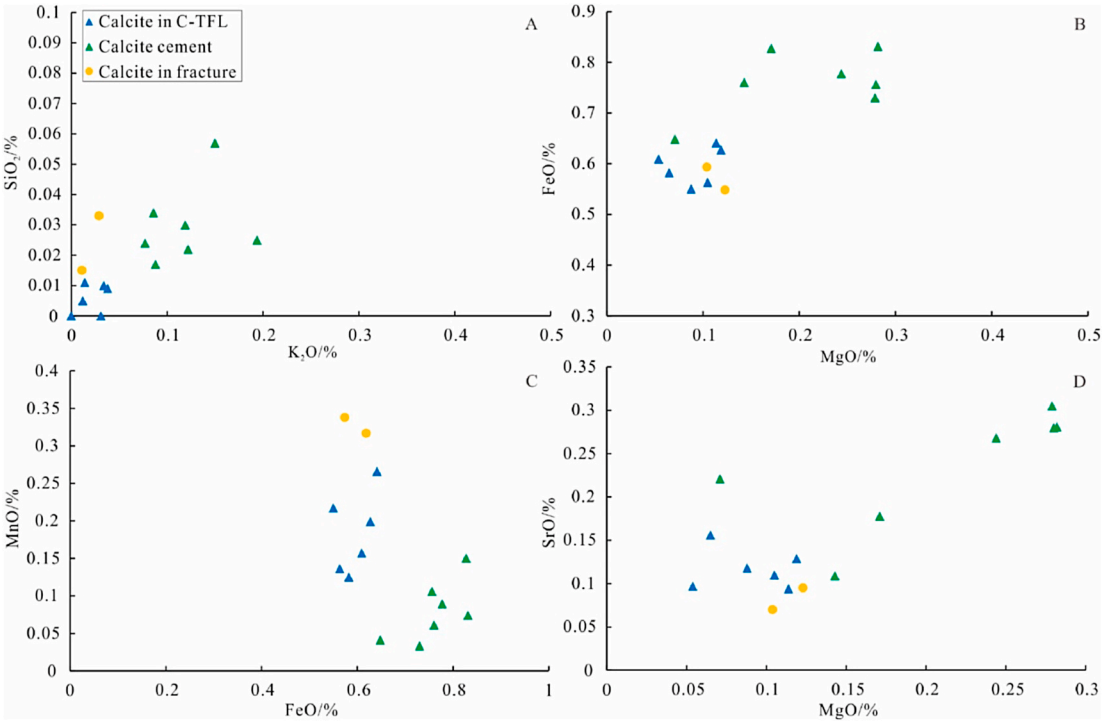

Fig. 14. Element correlation characteristics of calcite cements in the shale consisting of calcite-rich tufaceous lamina (C-TFL) and terrigenous felsic lamina (TL). (A) The correlation that K_2O content increases with increasing SiO_2 content of calcite cements. (B–D) There are positive correlations between the contents of FeO, MgO and SrO.

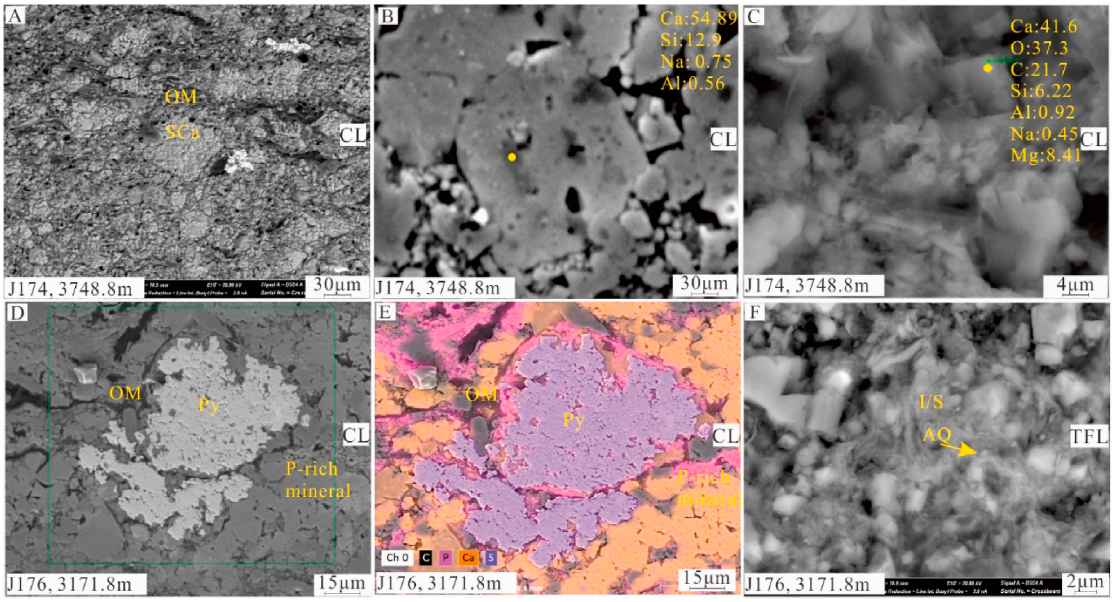

Fig. 15. Characteristics of calcite and silty-crystal calcites and massive pyrites in the shale consisting of calcareous lamina (CL) and tufaceous lamina (TFL). (A) BSE image showing silty-crystal calcites are composed of multiple micrite calcite; (B) SEM image showing dark parts of impurity minerals containing higher Si, Na, Al in silty-crystal calcites; (C) BSE image showing micrite dolomite are rich in elements of Mg, Si, Na, Al; (D) BSE image showing massive pyrites frequently coexists with P-rich minerals and are surrounded by organic matter; (E) EDS scanning showing the same area with (D); (F) BSE image showing P-bearing bioclasts. TFL = tufaceous lamina, CL = calcareous lamina, SCa = silty-crystal calcites, OM = organic matter, Py = pyrite, AQ = authigenic quartz.

and inorganic components generally coexist, resulting in complex organic-inorganic interactions during the diagenetic process (Cobbold et al., 2013; Milliken et al., 2016; Jin et al., 2020; Liu H et al., 2019). Fluid activities and mass transfer at the micro-scale cause mineral dissolution-precipitation and other diagenetic responses, which are of great significance to the formation of shale reservoirs (Mathia et al., 2016; Liang et al., 2018; Wang et al., 2019, 2023). The research results of the Lucaogou Formation shale indicate that there are diagenetic differences among three types of shales with different laminae combinations. For example, Type A shale is characterized by two-stage dolomite cementation (Fig. 3). Type B shale is characterized by strong calcite cementation (Fig. 5), and Type C shale is characterized by calcite

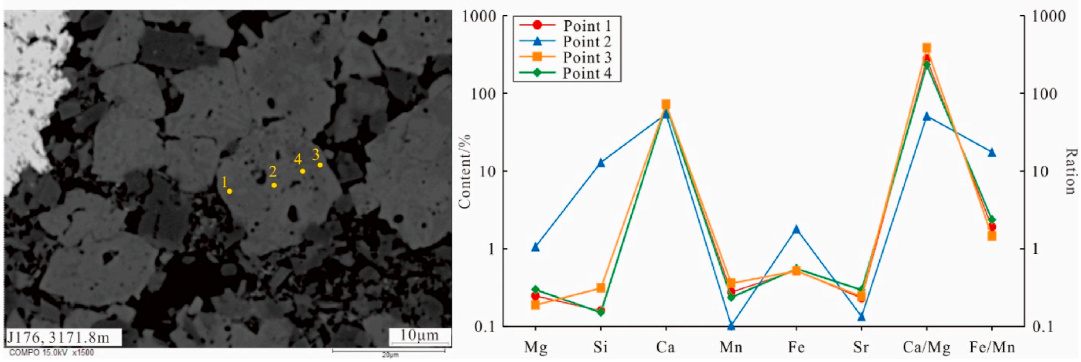

Fig. 16. Elemental geochemistry of the silty-crystal calcites in the shale consisting of calcareous lamina (CL) and tufaceous lamina (TFL).

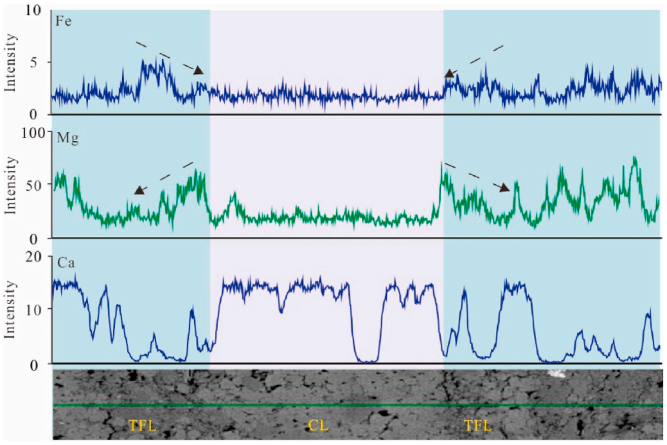

Fig. 17. Distribution characteristics of elements in the shale consisting of calcareous lamina (CL) and tufaceous lamina (TFL) by line scanning.

recrystallization (Fig. 6). The organic-inorganic interactions between different laminae are the key reason for the diagenetic variations (Schulz et al., 2016; Wu et al., 2017; Liang et al., 2018; Liu H et al., 2019; Han Y et al., 2019; Lin et al., 2021). In Type A shale, the organic acids generated by early maturation of the organic matter in the DL diffuse outward, causing recrystallization of micrite dolomite within the laminae and dolomite recrystallization in the TL to form I-stage dolomite (Fig. 18). As the organic matter further matures in the DL, sufficient organic acid and Ca and Mg rich fluid diffused into the TL. The surplus organic acids start dissolving the calcium-bearing feldspar, and the smectite undergoes transformation into illite (Fig. 8). These transformations provided a material source for the precipitation of stage II dolomite (Fig. 18). In Type B shale, the organic matter in the C-TFL released organic acids during early maturation. This leads to the dissolution of calcite fragments within the C-TFL and their diffusion to the adjacent TL, resulting in the dissolution of potassium feldspar (Lin et al., 2021). Subsequently, calcite-rich fluids in the C-TFL were gradually released to the adjacent TL. At the same time, the transformation of smectite to illite provided abundant ions (Stroker et al., 2013; Sun et al., 2020), leading to the

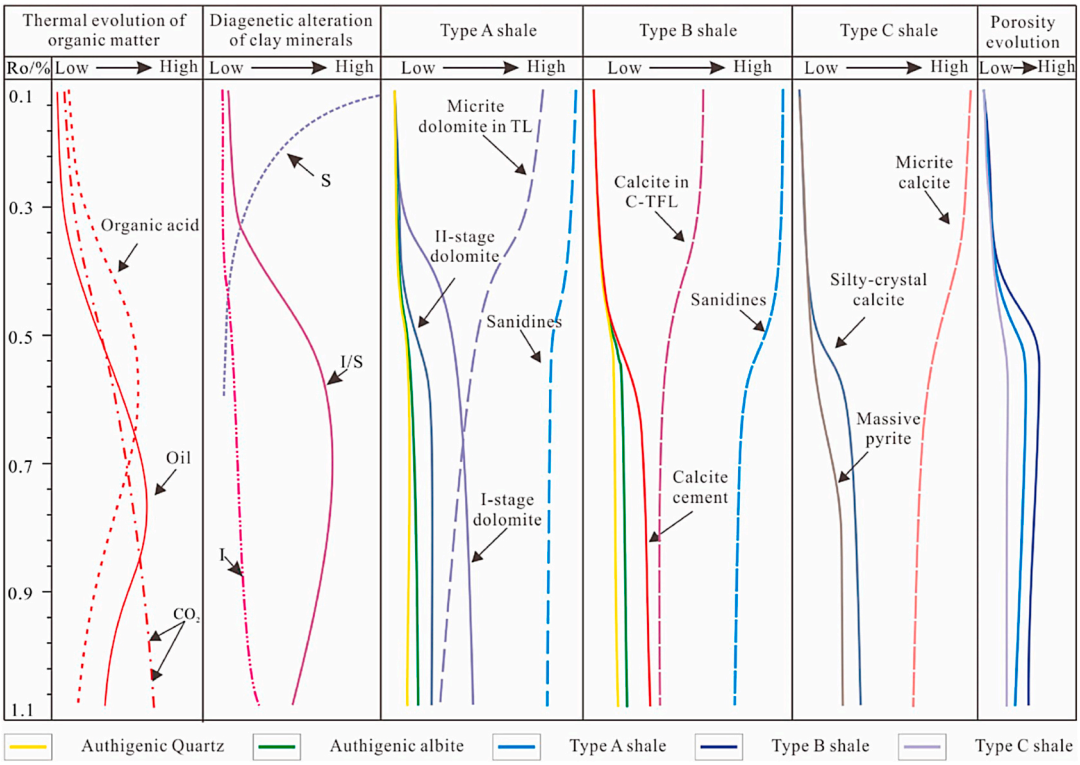

Fig. 18. The model of organic-inorganic interaction and shale oil reservoir formation in the Lucaogou formation shales.

formation of calcite cements in the TL (Fig. 18). In Type C shale, the thermal evolution of sulfur-bearing organic matter in the TFL produced acidic fluid. The acidic fluid caused the dissolution of micrite calcite in the CL near the laminae interface, removing toxic ions and impurities (Liang et al., 2018). Subsequently, the micrite calcite transformed into larger particles through recrystallization. Meanwhile, the sulfur-rich organic matter also drives the formation of massive pyrite (Khan et al., 2022), leading to the presence of pyrite and recrystallized calcite associated with organic matter (Fig. 18).

The dissolution and precipitation of carbonate minerals in the Lucaogou Formation shale indicate that the products of organic evolution play a role in the diagenesis of inorganic minerals. Additionally, the transfer and redistribution of diagenetic mass occur between adjacent laminae or within a lamina in a relatively closed diagenetic system (Fig. 18). The fluid originated from organic-rich laminae can remove toxic ions and impurities, promoting carbonate mineral recrystallization (Reddy, 2012; Liang et al., 2018), or diffuse into adjacent laminae, causing strong cementation (Fig. 18). In this process, the dissolution pores of feldspar and the recrystallization pores of carbonate, which are related to organic evolution, have provided a key space for shale oil in the Lucaogou formation shale (Fig. 18). However, carbonate minerals can also cause changes in the micro-scale pore structure and mechanical properties (Mathia et al., 2016; Liang et al., 2018; Wang et al., 2021). In type A shale, the content of dissolution pores was determined by the amount of micrite dolomite in the TL. In type B shale, the content of calcite fragments in adjacent C-TFL controls the degree of calcite cements in the TL, and therefore controls the content of residual dissolved pores of feldspar. In type C shale, the degree of calcite recrystallization affects the development of pores. In addition, the production of carbonate cements might make the shale more brittle, which is conducive to economically effective shale oil exploration (Han et al., 2019; Liu et al., 2020; Jin et al., 2020; Gou and Xu, 2023). To summarize, the redistribution of diagenetic materials through the organic-inorganic interaction between different component laminae within the enclosed shale is crucial for the formation of productive reservoirs.

6. Conclusions

The fine-grained sedimentary rocks of the Luchaogou Formation are complex. Three types of shale were observed: shale consist of dolomitic lamina and terrigenous felsic lamina (Type A shale), shale consist of calcite-rich tufaceous lamina and terrigenous felsic lamina (Type B shale), and shale consist of calcareous lamina and tufaceous lamina (Type C shale).

There are significant diagenetic differences among three types of shale. Type A shale is characterized by strong dolomite cementation, while type B shale is characterized by intense calcite cementation. Type C shale, on the other hand, is characterized by calcite recrystallization. Dolomite cements can be identified as Stage I dolomite, formed through the recrystallization of micrite dolomite, and Stage II dolomite, precipitated from adjacent dolomitic lamina. Calcite cements primarily originated from calcite fragments in adjacent calcite-rich tufaceous lamina. These processes are initiated by organic acids and carbonic acid. Moreover, the silty-crystal calcites mainly originated from the recrystallization of micrite calcite. This process involves the separation of toxic ions and impurities under the influence of organic acids from the adjacent TFL. Meanwhile, the formation of massive pyrite promoted this process.

The products of organic evolution in shale include hydrocarbons, acids, and CO_2, all of which contribute to the diagenesis of inorganic minerals. These organic-rich fluids promote the recrystallization of carbonate minerals within laminae or diffuse along the boundaries of laminae into adjacent layers, resulting in dense cementation. In the process, dissolution pores and intercrystalline pores created through recrystallization related to organic evolution, have played a crucial role in providing the necessary space for shale oil in the Lucaogou Formation shale. Therefore, the redistribution of diagenetic materials through the organic-inorganic interaction between adjacent laminae within the enclosed shale is crucial for reservoir formation.

CRediT authorship contribution statement

Ke Li: Writing – original draft. **Kelai Xi:** Writing – review & editing. **Yingchang Cao:** Writing – review & editing. **Xiang Shan:** Resources. **Miruo Lin:** Writing – review & editing, Methodology.

Declaration of competing interest

The authors declare that they have no known competing financial interests or personal relationships that could have appeared to influence the work reported in this paper.

Data availability

Data will be made available on request.

Acknowledgments

This study was co-supported by the National Natural Science Foundation of China (Grant No. 42072161), Taishan Scholars Program (tsqn202306125), Innovation Research Group of the Natural Fund Committee (Grant No. 41821002) and Fundamental Research Funds for the Central Universities (22CX07008A). We are also grateful to the Xinjiang Oilfield Company, PetroChina, for providing their inhouse database and permission to publish.

References

Barbera, G., Critelli, S., Mazzoleni, P., 2011. Petrology and geochemistry of cretaceous sedimentary rocks of the monte soro unit (Sicily, Italy): constraints on weathering, diagenesis and provenance. J. Geol. 119 (1), 51–68.

Campo, M.D., Papa, C.D., Nieto, F., Hongn, F., Petrinovic, I., 2010. Integrated analysis for constraining palaeoclimatic and volcanic influences on clay-mineral assemblages in orogenic basins (Palaeogene Andean foreland, Northwestern Argentina). Sediment. Geol. 228 (3–4), 98–112.

Caracciolo, L., Arribas, J., Ingersoll, R.V., Critelli, S., 2014. The diagenetic destruction of porosity in plutoniclastic petrofacies: the Miocene Diligencia and Eocene Maniobra formations, Orocopia Mountains, southern California, USA. In: Scott, R.A., Smyth, H. R., Morton, A.C., Richardson, N. (Eds.), Sediment Provenance Studies in Hydrocarbon Exploration and Production, vol. 386. Geological Society, London, Special Publication, pp. 49–62.

Civitelli, M., Ravidà, D.C.G., Borrelli, M., Criniti, S., Falsetta, E., 2023. Diagenesis and petrophysics of Miocene sandstones within southern Apennines foreland, Italy. Mar. Petrol. Geol. 155, 106411.

Cobbold, P.R., Zanella, A., Rodrigues, N., Løseth, H., 2013. Bedding-parallel fibrous veins (beef and cone-in-cone): worldwide occurrence and possible significance in terms of fluid overpressure, hydrocarbon generation and mineralization. Mar. Petrol. Geol. 43, 1–20.

Criniti, S., Martín-Martín, M., Martín-Algarra, A., 2023. New constraints for the western paleotethys paleogeographypaleotectonics derived from detrital signatures: malaguide carboniferous culm cycle (betic Cordillera, S Spain). Sediment. Geol., 106534

Critelli, S., Nilsen, T.H., 1996. Petrology and diagenesis of the eocene butano sandstone, La honda basin, California. J. Geol. 104 (3), 295–315.

Critelli, S., Perri, F., Arribas, J., Herrero, M.J., 2018. Sandstone detrital modes and diagenetic evolution of Mesozoic continental redbeds from western-central circum-Mediterranean orogenic belts. In: Ingersoll, R.V., Lawton, T.F., Graham, S. (Eds.), Tectonics, Sedimentary Basins and Provenance: A Celebration of William R. Dickinson's Career, vol. 540. Geological Society of America Special, pp. 119–132.

Dowey, P.J., Taylor, K.G., 2020. Diagenetic mineral development within the upper jurassic haynesville-bossier shale, USA. Sedimentology 67, 47–77.

Edery, Y., Scher, H., Berkowitz, B., 2011. Dissolution and precipitation dynamics during dedolomitization. Water Resour. Res. 47, W08535.

Gou, Q., Xu, S., 2023. The controls of laminae on lacustrine shale oil content in China: a review from generation, retention, and storage. Energies 16, 1987.

Han, J., Daigle, H., Milliken, K.L., Hayman, N.W., 2020. Porosity-deformation relationships in organic-rich shale. In: Camp, W.K., Milliken, K.L., Taylor, K., Fishman, N., Hackley, P.C., Macquaker, J.H.S. (Eds.), Mudstone Diagenesis: Research Perspectives for Shale Hydrocarbon Reservoirs, Seals, and Source Rocks, vol. 120, pp. 149–164.

Han, Y., Horsfield, B., Mahlstedt, N., Wifth, R., Curry, D.J., LaReau, H., 2019. Factors controlling source and reservoir characteristics in the Niobrara shale oil system, Denver Basin. AAPG (Am. Assoc. Pet. Geol.) Bull. 103 (9), 2045–2072.
Hart, B.S., Macquaker, J.H.S., Taylor, K.G., 2013. Mudstone ("shale") depositional and diagenetic processes: implications for seismic analyses of source-rock reservoirs. Interpretation 1 (1), B7–B26.
Hayashi, K.I., Fujisawa, H., Holland, H.D., Ohmoto, H., 1997. Geochemistry of~ 1.9 Ga sedimentary rocks from northeastern Labrador, Canada. Geochem. Cosmochim. Acta 61 (19), 4115–4137.
Hu, T., Pang, X., Jiang, F., Wang, Q., Liu, X., Wang, Z., Jiang, S., Wu, G., Li, C., Xu, T., Li, M., Yu, J., Zhang, C., 2021. Movable oil content evaluation of lacustrine organic-rich shales: methods and a novel quantitative evaluation model. Earth Sci. Rev. 214, 103545.
Jin, Z., Nie, H., Liu, Q., Zhao, J., Wang, R., Sun, C., Wang, G., 2020. Coevolutionary dynamics of organic-inorganic interactions, hydrocarbon generation, and shale gas reservoir preservation: a case study from the upper ordovician Wufeng and lower Silurian Longmaxi formations, fuling shale gas field, eastern Sichuan basin. Geofluids 2020, 6672386.
Johannes, W., Puhan, D., 1971. The calcite-aragonite transition, reinvestigated. Mar. Petrol. Geol. 31, 28–38.
Khan, D., Qiu, L., Liang, C., Mirza, K., Rehman, S.U., Han, Y., Hannan, A., Kashif, M., Kra, K.L., 2022. Genesis and distribution of pyrite in the lacustrine shale: evidence from the Es3x shale of the eocene Shahejie formation, Zhanhua sag, east China. ACS Omega 7 (1), 1244–1258.
Lai, J., Wang, G., Ran, Y., Zhou, Z., Cui, Y., 2016. Impact of diagenesis on the reservoir quality of tight oil sandstones: the case of Upper Triassic Yanchang Formation Chang 7 oil layers in Ordos Basin, China. J. Pet. Sci. Eng. 145, 54–65.
Lazar, O.R., Bohacs, K.M., Macquaker, J., Schieber, J., Demko, T.M., 2015. Capturing key attributes of fine-grained sedimentary rocks in outcrops, cores, and thin sections: nomenclature and description guidelines. J. Sediment. Res. 85 (3), 230–246.
Liang, C., Cao, Y., Liu, K., Jiang, Z., Wu, J., Hao, F., 2018. Diagenetic variation at the lamina scale in lacustrine organic-rich shales: implications for hydrocarbon migration and accumulation. Geochem. Cosmochim. Acta 229, 112–128.
Li, H., Liu, Y., Yang, K., Liu, Y., Niu, Y., 2021. Hydrothermal mineral assemblages of calcite and dolomite–analcime-pyrite in Permian lacustrine Lucaogou mudstones, eastern Junggar Basin, Northwest China. Min. Pet. 115, 63–85.
Li, K., Xi, K., Cao, Y., Wang, Y., Lin, M., 2023. Genesis of granular calcite in lacustrine fine-grained sedimentary rocks and its indication to volcanic-hydrothermal events: a case study of Permian Lucaogou Formation in Jimusar Sag, Junggar Basin, NW China. Petrol. Explor. Dev. 50 (3), 615–627.
Li, Q., You, X., Jiang, Z., Wu, S., Zhang, R., 2020. The origins of carbonate minerals of a source-controlled lacustrine carbonate succession in the Shulu sag, Bohai Bay Basin: implications for porosity development and paleoenvironment. Mar. Petrol. Geol. 122, 104673.
Li, W., Kuang, Y., Lu, S., Cheng, Z., Xue, H., Shi, L., 2019. Porosity enhancement potential through dolomite mineral dissolution in the shale reservoir: a case study of an argillaceous dolomite reservoir in the Jianghan basin. Energy Fuel. 33 (6), 4857–4864.
Li, Y., Chen, J., Elsworth, D., Pan, Z., Ma, X., 2022. Nanoscale mechanical property variations concerning mineral composition and contact of marine shale. Geosci. Front. 13 (4), 101405.
Lin, M., Xi, K., Cao, Y., Liu, Q., Zhang, Z., Li, K., 2021. Petrographic features and diagenetic alteration in the shale strata of the permian lucaogou formation, Jimusar Sag, Junggar basin. J. Pet. Sci. Eng. 203 (1), 108684.
Liu, B., Wang, S., Ke, X., Fu, X., Liu, X., Bai, Y., Pan, Z., 2020. Mechanical characteristics and factors controlling brittleness of organic-rich continental shales. J. Petrol. Sci. Eng. 194, 107464.
Liu, H., Zhang, S., Song, G., Wang, X., Teng, J., Wang, M., Bao, Y., Yao, S., Wang, W., Zhang, S., Hu, Q., Fang, Z., 2019a. Effect of shale diagenesis on pores and storage capacity in the Paleogene Shahejie formation, Dongying depression, Bohai Bay basin, east China. Mar. Petrol. Geol. 103, 738–752.
Liu, Y., Ma, K., Hou, J., Yan, L., Chen, F., 2019b. Diagenetic controls on the quality of the middle permian Lucaogou Formation tight reservoir, southeastern Junggar Basin, northwestern China. J. Asian Earth Sci. 178, 139–155.
Machel, H.G., 2001. Bacterial and thermochemical sulfate reduction in diagenetic settings—old and new insights. Sediment. Geol. 140 (1–2), 143–175.
Mathia, E.J., Bowen, L., Thomas, K.M., Aplin, A.C., 2016. Evolution of porosity and pore types in organic-rich, calcareous, Lower Toarcian Posidonia Shale. Mar. Petrol. Geol. 75, 117–139.
Milliken, K.L., Ergene, S.M., Ozkan, A., 2016. Quartz types, authigenic and detrital, in the upper cretaceous eagle ford formation, south Texas, USA. Sediment. Geol. 339, 273–288.
Parcerisa, D., Gómez-Gras, D., Travé, A., Martin-Martin, J.D., Maestro, E., 2006. Fe and Mn in calcites cementing red beds: a record of oxidation-reduction conditions -: examples from the Catalan Coastal Ranges (NE Spain). J. Geochem. Explor. 89, 318–321.
Qu, C., Qiu, L., Yang, Y., Yu, K., Tang, L., Wan, M., 2019. Environmental response of the permian volcanism in Lucaogou Formation in Jimusar Sag, Junggar Basin, northwest China. Seismol. Geol. 41 (3), 789–802 (in Chinese with English abstract).
Reddy, M.M., 2012. Calcite growth-rate inhibition by fulvic acid and magnesium ion-Possible influence on biogenic calcite formation. J. Cryst. Growth 352 (1), 151–154.
Schulz, H.M., Wirth, R., Schreiber, A., 2016. Organic-inorganic rock-fluid interactions in stylolitic micro-environments of carbonate rocks: a FIB-TEM study combined with a hydrogeochemical modelling approach. Geofluids 16, 909–924.
Stroker, T.M., Harris, N.B., Elliott, W.C., Wampler, J.M., 2013. Diagenesis of a tight gas sand reservoir: upper cretaceous mesaverde Group, Piceance basin, Colorado. Mar. Petrol. Geol. 40, 48–68.
Sun, L., Zhong, J., Hao, B., Ge, Y., Swennen, R., 2020. Sedimentological and diagenetic control on the reservoir quality of deep-lacustrine sedimentary gravity flow sand reservoirs of the Upper Triassic Yanchang Formation in Southern Ordos Basin, China. Mar. Petrol. Geol. 112, 104050.
Thyne, G., Boudreau, B.P., Ramm, M., Midtbo, R.E., 2001. Simulation of potassium feldspar dissolution and illitization in the Statfjord formation, north Sea. AAPG (Am. Assoc. Pet. Geol.) Bull. 85 (4), 621–635.
Tobia, F.H., 2018. Stable isotope and rare earth element geochemistry of the Baluti carbonates (Upper Triassic), Northern Iraq. Geoences J. 22 (6), 975–987.
Wang, C., Zhang, B., Hu, Q., Shu, Z., Sun, M., Bao, H., 2019. Laminae characteristics and influence on shale gas reservoir quality of lower Silurian Longmaxi Formation in the Jiaoshiba area of the Sichuan Basin, China. Mar. Petrol. Geol. 109, 839–851.
Wang, M., Chen, Y., Song, G., Steele-Macinnis, M., Liu, Q., Wang, X., Zhang, X., Zhao, Z., Liu, W., Zhang, H., Zhou, Z., 2018. Formation of bedding-parallel, fibrous calcite veins in laminated source rocks of the Eocene Dongying Depression: a growth model based on petrographic observations. Int. J. Coal Geol. 200, 18–35.
Wang, T., Wang, Q., Lu, H., Peng, P., Zhan, X., 2021. Understanding pore evolution in a lacustrine calcareous shale reservoir in the oil window by pyrolyzing artificial samples in a semi-closed system. J. Pet. Sci. Eng. 200, 108230.
Wang, Y., Xu, S., Hao, F., Zhang, B., Shu, Z., Guo, Q., Liu, Y., Cong, F., 2023. Multiscale petrographic heterogeneity and their implications for the nanoporous system of the Wufeng-Longmaxi shales in Jiaoshiba area, Southeast China: response to depositional-diagenetic process. GSA Bullet. 132, 1704–1721.
Wu, H., Hu, W., Tang, Y., Cao, J., Wang, X., Wang, Y., Kang, X., 2017. The impact of organic fluids on the carbon isotopic compositions of carbonate-rich reservoirs: case study of the Lucaogou Formation in the Jimusaer Sag, Junggar Basin, NW China. Mar. Petrol. Geol. 85, 136–150.
Wu, H., Hu, W., Cao, J., Wang, X., Wang, X., Liao, Z., 2016. A unique lacustrine mixed dolomitic-clastic sequence for tight oil reservoir within the middle permian lucaogou formation of the junggar basin, nw China: reservoir characteristics and origin. Mar. Petrol. Geol. 76, 115–132.
Xi, K., Cao, Y., Liu, K., Yuan, G., Zhu, R., Zhao, Y., Hellevang, H., 2019. Geochemical constraints on the origins of calcite cements and their impacts on reservoir heterogeneities: a case study on tight oil sandstones of the Upper Triassic Yanchang Formation, southwestern Ordos Basin, China. AAPG (Am. Assoc. Pet. Geol.) Bull. 103 (10), 2447–2485.
Xiong, Yijun, Guilbaud, R., Peacock, C.L., Cox, R.P., Canfield, D.E., Krom, M.D., Poulton, S.W., 2019. Phosphorus cycling in Lake Cadagno, Switzerland: a low sulfate euxinic ocean analogue. Geochem. Cosmochim. Acta 251, 116–135.
Xu, Y., Lun, Z., Pan, Z., Wang, H., Zhou, X., Zhao, C., Zhang, D., 2022. Occurrence space and state of shale oil: a review. J. Pet. Sci. Eng. 211, 110183.
Yang, X., Yan, D., Wei, X., Zhang, L., Zhang, B., Xu, H., Gong, Y., He, J., 2018. Different formation mechanism of quartz in siliceous and argillaceous shales: a case study of Longmaxi Formation in South China. Mar. Petrol. Geol. 94, 80–94.
Yuan, G., Cao, Y., Zan, N., Schulz, H.M., Gluyas, J., Hao, F., Jin, Q., Liu, K., Wang, Y., Chen, Z., Jia, Z., 2019. Coupled mineral alteration and oil degradation in thermal oil-water-feldspar systems and implications for organic-inorganic interactions in hydrocarbon reservoirs. Geochem. Cosmochim. Acta 248, 61–87, 2019.
Yoon, H., Ingraham, M.D., Grigg, J., Rosandick, B., Moaley, P., Rinehart, A., Mook, W.M., Dewer, T., 2020. Impact of depositional and diagenetic heterogeneity on multiscale mechanical behavior of mancos shale, New Mexico and Utah, USA. In: Camp, W.K., Milliken, K.L., Taylor, K., Fishman, N., Hackley, P.C., Macquaker, J.H.S. (Eds.), Mudstone Diagenesis: Research Perspectives for Shale Hydrocarbon Reservoirs, Seals, and Source Rocks, vol. 120, pp. 121–148.
Zhang, B., Wen, S., Yang, K., Ma, K., Wang, P., Xu, C., Gao, G., 2023. Diagenetic evolution sequence and pore evolution characteristics: study on marine-continental transitional facies shale in southeastern Sichuan basin. Minerals 13, 1451.
Zhang, J., Jiang, Z., Liu, P., Kong, X., Ge, y., 2022. Deposition mechanism and geological assessment of continental ultrafine-grained shale oil reservoirs. Acta Pet. Sin. 43 (2), 234–249 (in Chinese with English abstract).
Zhou, L., Pang, X., Wu, L., Kuang, L., Pang, H., Jiang, F., Bai, H., Peng, J., Pan, Z., Zheng, D., 2017. Petroleum generation and expulsion in middle Permian Lucaogou Formation, Jimusar Sag, Junggar Basin, northwest China: assessment of shale oil resource potential. Geol. J. 52 (6), 1032–1048.
Zou, C., Zhu, R., Chen, Z., Ogg, J.G., Wu, S., Dong, D., Qiu, Z., Wang, Y., Wang, L., Lin, S., Cui, J., Su, L., Yang, Z., 2019. Organic-matter-rich shales of China. Earth Sci. Rev. 189, 51–78.
Zhao, W., Hu, S., Hou, L., Yang, T., Li, X., Guo, B., Yang, Z., 2020. Types and resource potential of continental shale oil in China and its boundary with tight oil. Petrol. Explor. Dev. 47 (1), 1–10.